

Review

Review of Laser-Generated Ultrasound Transmitters and Their Applications to All-Optical Ultrasound Transducers and Imaging

Sung-Liang Chen ^{1,2}

¹ Electrical and Computer Engineering, University of Michigan-Shanghai Jiao Tong University Joint Institute, Shanghai Jiao Tong University, Shanghai 200240, China; sungliang.chen@sjtu.edu.cn; Tel.: +86-21-3420-6045

² State Key Laboratory of Advanced Optical Communication Systems and Networks, Shanghai Jiao Tong University, Shanghai 200240, China

Academic Editor: Kohji Masuda

Received: 19 November 2016; Accepted: 19 December 2016; Published: 28 December 2016

Abstract: Medical ultrasound is an imaging technique that utilizes ultrasonic signals as information carriers, and has wide applications such as seeing internal body structures, finding a source of a disease, and examining pregnant women. The most commonly used ultrasonic transducer today is based on piezoelectricity. The piezoelectric transducer, however, may have a limited bandwidth and insufficient sensitivity for reduced element size. Laser-generated ultrasound (LGUS) technique is an effective way to resolve these issues. The LGUS approach based on photoacoustic effect is able to greatly enhance the bandwidth of ultrasound signals and has the potential for high-resolution imaging. High-amplitude LGUS could also be used for therapy to accomplish high precision surgery without an incision. Furthermore, LGUS in conjunction with optical detection of ultrasound allows all-optical ultrasound imaging (i.e., ultrasound is generated and received optically). The all-optical platform offers unique advantages in providing high-resolution information and in facilitating the construction of miniature probes for endoscopic ultrasound. In this article, a detailed review of the recent development of various LGUS transmitters is presented. In addition, a recent research interest in all-optical ultrasound imaging, as well as its applications, is also discussed.

Keywords: ultrasound imaging; laser ultrasonics; laser-ultrasound transducer; laser-generated focused ultrasound; all-optical ultrasound imaging

1. Introduction

Ultrasound, defined as sound with frequencies from 20 kHz to several GHz, has demonstrated broad applications in medical imaging [1], material science, physics, chemistry, and nanotechnology. In classical medical ultrasound (also known as ultrasonography), an ultrasound pulse is transmitted into the body and the pulse is reflected due to the interfaces between tissues with different acoustic impedances as image contrast. The echo pulse carries back physiological and pathological information inside tissues. Especially, high-frequency ultrasound with frequencies >20 MHz is useful for high-resolution (<100 μm) biomedical applications such as endoscopic imaging [2], ophthalmology [3], intravascular imaging [4] and dermatology [5]. Magnetic resonance imaging (MRI) systems continue to enhance the resolution up to ~500 μm [6]. However, routine interventional procedures are restricted due to the high expense of MRI in both the initial investment and the upkeep. Furthermore, MRI has limited temporal resolution, which prohibits its use in fast imaging and rapid diagnosis. X-ray computed tomography is a relatively affordable modality with high resolution of ~400 μm [7], but it relies on ionizing radiation, making it unsafe for medical monitoring. Optical method is a promising approach for biomedical imaging [8]. Optical coherence tomography (OCT) is an optical technique

that can support real-time imaging with high resolution ($<10 \mu\text{m}$) [9]; however, OCT suffers from limited penetration depth ($<1 \text{ mm}$). Nowadays, the majority of ultrasound imaging systems are safe and portable, and can provide high frame rates beyond 25 frames per second, the threshold for real-time display. It is worth mentioning that photoacoustic imaging derived from ultrasonography is an emerging modality that relies on laser pulses directed on tissues to produce ultrasound [10–12]. Photoacoustic imaging can, therefore, possess the penetration depth of ultrasound while maps the optical absorption of tissues instead.

Presently, piezoelectric transducers are the principle measure to produce biomedical ultrasound for imaging and therapy applications [13,14]. However, high-resolution ultrasound imaging ($<100 \mu\text{m}$) is restricted due to the limited bandwidth of ultrasonic signals generated by the piezoelectric effect. High intensity focused ultrasound (HIFU) is valuable for therapeutic applications [15,16]. Its applications featuring high-frequency ultrasound for precision therapy also face challenges due to the frailty of piezoelectric materials and impedance mismatch for a large aperture [17]. Capacitive micromachined ultrasonic transducers (CMUTs) are an alternative technique that is promising to produce broadband ultrasound pulses [18–21], yet there exist technical challenges in realizing two-dimensional (2D) high-frequency CMUT arrays [22]. Laser-generated ultrasound (LGUS) has been investigated over decades [23–25]. LGUS is with a recent enthusiasm in high-frequency ultrasound and HIFU. LGUS transmitters usually consist of optical absorbers for efficient conversion of light energy into heat, and surrounding media with high coefficients of thermal expansion for generating high-intensity ultrasound. Based on photoacoustic effect, the LGUS transmitters generate ultrasound pulses following the laser profile. If a short laser is employed, short ultrasound pulses in the scale of nanoseconds can be produced. Thus, it is a relatively simple method to create a broadband and high-frequency ultrasound signal. Efforts have been made aiming to optimize laser-ultrasound transduction efficiency in recent years, especially for high-frequency ultrasound generation. Laser-ultrasound transduction efficiency can be described by $p_0 = \Gamma A_e$ [26], where p_0 is the local pressure immediately after the laser radiation; $\Gamma = (\beta v_s^2)/C_p$ is defined as the Grueneisen coefficient, β is the thermal coefficient of volume expansion, v_s is the speed of sound, and C_p is the specific heat; $A_e = \mu_a F$ is the volumetric optical absorption, where μ_a is the optical absorption coefficient and F is the optical fluence. High optical absorption ensures high optical energy density deposited on the absorber, low specific heat provides high temperature rise under the same optical absorption, and large thermal coefficient of volume expansion produces strong pressure under the same temperature rise. (i) Materials with high optical absorption coefficient and low specific heat to reach local high temperature in the laser irradiation region are investigated. (ii) Absorbing materials with a unique spatial configuration such as nanoscale composition have been chosen to allow fast heat transfer into the expanding surroundings and thus the generation of high-frequency ultrasound. (iii) Polydimethylsiloxane (PDMS) has been considerably adopted as an attractive expanding matter in virtue of its high coefficients of thermal expansion [27]. LGUS transmitters are favorable for high-frequency arrays for high-resolution ultrasound imaging compared with traditional piezoelectric ultrasound transducers [28,29]. In addition, efficient and broadband laser-generated focused ultrasound enables broad HIFU applications such as high-precision therapy [30] and micro-droplet ejection [31]. Furthermore, the advantage of contactless excitation furnished by LGUS transmitters permits unique applications that may not be attained by conventional ultrasound transmitters.

Based on optical generation and detection of ultrasound, all-optical ultrasound transducers (AOUSTs) and their application to all-optical ultrasound imaging (AOUSI) are realized. As mentioned above, LGUS transmitters can generate a broadband and high-frequency ultrasound signal. For optical detection of ultrasound (ODUS), optical resonance can be used to realize sensitive and broadband ultrasound detection. There are several types of ODUS detectors such as microring resonators [32], Fabry–Perot (FP) etalons [33], and Mach–Zehnder interferometers [34]. The optical detection platform intrinsically facilitates broadband ultrasound detection up to hundreds of MHz [32,35]. Therefore, AOUSTs hold the promise for high-resolution ultrasound imaging compared with piezoelectric

transducers. In addition, unlike the piezoelectric transducer, the detection sensitivity of ODUS detectors is inherently independent of their active area, which is optically defined on an order of microns. Although the reduced optical active area may impair the optical property such as quality factors and thus the ultrasound detection sensitivity [36,37], there exist approaches to recover the degraded optical property [38]. High sensitivity is thus preserved with small active area. On the other hand, the LGUS transmitters can be realized with a similar size, for example, using a point-like laser source or light-absorbing material for ultrasound excitation. Such features can be utilized to construct a miniature AOUST probe without sacrificing its sensitivity, which facilitates a range of applications such as endoscopic ultrasound imaging and minimally invasive clinical procedures. The possibility of noncontact operation of AOUSTs exhibits another advantage over conventional transducers.

In this review article, various progress of LGUS transmitters and AOUSTs in recent years is presented. In Section 2, the development of LGUS transmitters is described. A variety of absorbers such as carbon nanotubes (CNTs) and gold (Au) nanoparticles (NPs) (AuNPs) are employed for efficient photoacoustic transmission. New design and structures for LGUS transmitters in order to facilitate specific applications such as high-precision therapy are discussed. In Section 3, the recent implementation of AOUSTs is introduced. The performance of AOUST imaging systems and their applications are also reported. At the end, a summary and an outlook about LGUS transmitters and AOUST are provided.

2. Laser-Generated Ultrasound

With the development of advanced ultrasound technologies, LGUS technique has played an important role in biomedical ultrasound imaging and industrial nondestructive evaluation. There are various investigations on LGUS transmitters including mathematical modeling and analysis, effective absorbing materials, fiber-optic transmitters for extensive applications, and ultrasound beam focusing and shaping (as will be discussed in Sections 2.2.2 and 2.2.3). Efficient LGUS transmission could significantly increase the pressure, effectively improve penetration depth, and even provide useful thermal and mechanical effects on tissues. High-efficiency LGUS transmission strongly demands the novel materials with high laser absorption, low heat capacity, and large thermoelastic expansion. For instance, an AuNPs–PDMS nanocomposite is utilized to enhance the efficiency of LGUS transmission, which has three orders of magnitude improvement compared with an aluminum (Al) thin film [39]. The recent interest in CNT materials has led to exceptional transduction performance of LGUS transmitters and has expanded the application of LGUS to therapeutic ultrasound [30]. New materials as LGUS transmitters are typically tested in the form of a thin film during initial exploration. To meet specific applications, further development is required. LGUS transmitters built on optical fibers featuring a compact size facilitates interventional ultrasound applications such as intravascular ultrasound (IVUS) imaging. More recently, high-power laser-generated focused ultrasound based on an acoustic lens has drawn surging interest, which has the potential to open up promising applications in therapeutic ultrasound. Ultrasound beam focusing and beam shaping may also be realized through array implementation of LGUS transmitters. Traditional ultrasound transducers face challenges with modern applications, while AOUSTs combining LGUS transmitters and ODUS detectors fill the gap by unique performances such as broad bandwidth and possibly noncontact characteristics. Besides medical imaging and therapy, LGUS technique also demonstrates broad applications for material characterization and evaluation such as PDMS thin film characterization, crack inspection, and investigation of phase transitions in metals (as will be discussed in Section 2.3).

2.1. Absorptive Materials

In this subsection, a detailed review of various light-absorbing materials for LGUS transmitters is presented. By virtue of its high thermoelastic expansion [40], PDMS, which is not considered as a type of absorber, is favorably mixed with the absorber to enhance LGUS efficiency. A summary of the

attributes of LGUS transmitters is provided in Table A1 in Appendix, where several types of absorbers are used.

2.1.1. Metallic Absorbers

The LGUS by laser irradiation on metals was first proposed by White in 1963 [41], which can be driven by the ablation and the thermoelastic effect. The ablation has to melt the material resulting in plasma formation by applying a large optical power, while the thermoelastic effect does not. Thus, the thermoelastic effect is more desired in practical applications. A thin metal film irradiated by a short pulsed laser beam is capable of inducing a broadband acoustic wave. Furthermore, the adjacent materials of the thin metal film should also be considered for efficient generation of high-frequency ultrasound [42].

AuNPs are used to optically generate high-frequency ultrasound. There are several examples. (i) A two-dimensional Au nanostructure consisting of AuNPs sandwiched between a substrate and a 4.5- μm PDMS layer is used to generate ultrasound in the 100 MHz regime [43]. Scanning electron microscope (SEM) picture of the nanostructure is shown in Figure 1. The 2D nanostructure also facilitates the construction of LGUS array transmitters for high-frequency ultrasound imaging. (ii) A one-pot synthesized AuNPs–PDMS nanocomposite for high-amplitude ultrasound generation is demonstrated [39]. The efficiency is optimized through the investigation on various concentrations and thickness of the nanocomposite film. Compared with the pressure generated by an Al thin film, the AuNPs–PDMS transmitter has shown increased efficiency by three orders of magnitude. (iii) The process of heating of AuNPs is studied numerically by finite element analysis [44]. The results can also provide useful guidance for other applications such as photothermal therapy. (iv) AuNPs are tested for fabricating fiber-optic LGUS transmitters [45–47]. AuNPs can be coated on the end face [45,46] or on the sidewall [47] of optical fibers. (v) A novel one-dimensional photonic crystal-metallic structure is proposed for complete absorption of optical energy at specific wavelengths for efficient LGUS transmission [40].

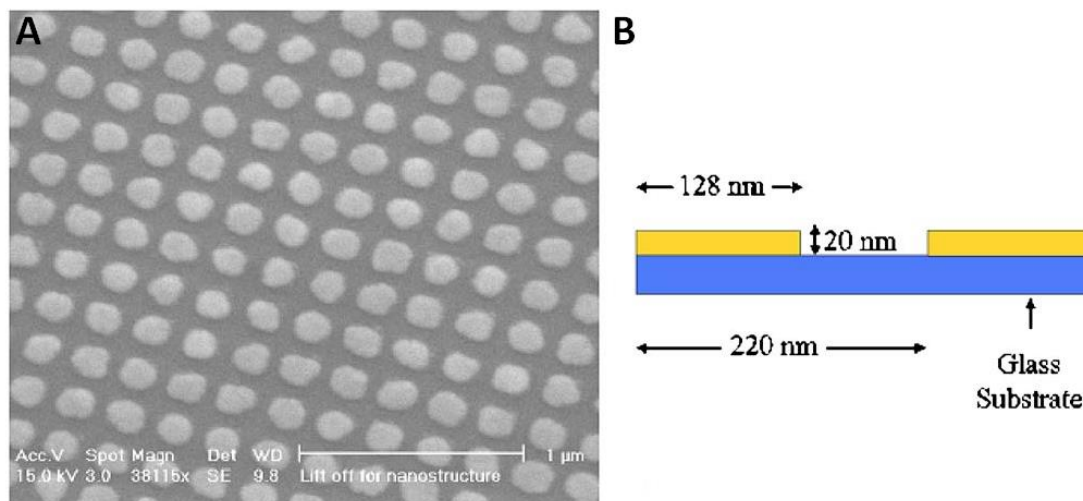


Figure 1. (A) Scanning electron microscope (SEM) picture of the two-dimensional (2D) Au nanostructure (top view); and (B) schematic of the 2D Au nanostructure on a substrate (side view). Reproduced with permission from [43], AIP Publishing, 2006.

Besides AuNPs, there are several studies on other metals for LGUS transmitters. (i) The laser-generated surface acoustic waves in an Al plate are studied by the finite element model [48]. It is found that the laser parameters are influential factors on the induced ultrasound waves. (ii) Thin Al film coated with reduced graphene oxide (rGO) for its high thermal conductivity is an effective LGUS transmitter, which shows a 64 times enhancement compared to an Al-along transmitter [49]. (iii) The

Al states such as the dynamics of temperature and pressure can be studied by heating a submicron Al film with high power nanosecond laser pulses [50]. (iv) Nanostructured germanium (Ge) overlaid with PDMS is fabricated for highly-efficient generation of high-frequency ultrasound [51]. The substrate can be chosen arbitrarily in the fabrication process, allowing flexible applications.

2.1.2. Carbon-Based Absorbers

Carbon-based materials are used to realize efficient and broadband LGUS transmission. They often, but not always, show higher LGUS transmission efficiency than metal-based materials. (i) Carbon black (CB)–PDMS is used to produce high-frequency ultrasound [52]. It has the potential to generate ultrasound with broad bandwidth above 100 MHz. The amplitude of ultrasound produced by CB–PDMS is slightly less than that by AuNPs–PDMS [43]. (ii) CNT nanocomposites are demonstrated as highly-efficient and high-frequency LGUS transmitters [30,53–55]. The CNT nanocomposite shows five times enhancement compared with the above-mentioned 2D AuNPs nanocomposite with the same polymer PDMS [43] and a broad bandwidth up to 120 MHz. The fast heat transition due to the nanoscale dimension of the CNT permits efficient generation of high-frequency ultrasound. Such advantage is shared in AuNPs. On the other hand, the exceptional thermal conductivity of the CNT facilitates better heat conduction, leading to the increased efficiency compared with AuNPs. Furthermore, the CNT has a high damage threshold, allowing generation of stronger pressure. (iii) Carbon nanofibers (CNFs)–PDMS thin films are also investigated [56]. Under 532-nm pulsed laser excitation with the laser fluence of 3.7 mJ/cm², the acoustic pressure of 12 MPa is achieved. (iv) More recently, candle soot carbon NPs (CSNPs)–PDMS nanocomposites are explored [57]. Figure 2 shows SEM pictures of CNTs, CNFs and CSNPs used in References [55–57], respectively. The ratio of photoacoustic conversion efficiency for CSNPs–PDMS, CNFs–PDMS, CNTs–PDMS, and CB–PDMS is 13:4.9:4.1:1 [57]. The unprecedented LGUS transmission performance by CSNPs–PDMS nanocomposites shows the promise for ultrasound therapeutic applications. (v) Besides the carbon NPs, graphite powder is explored for fiber-optic LGUS transmitters [58], where efficient and distributive ultrasound can be generated at specific locations along the fiber.

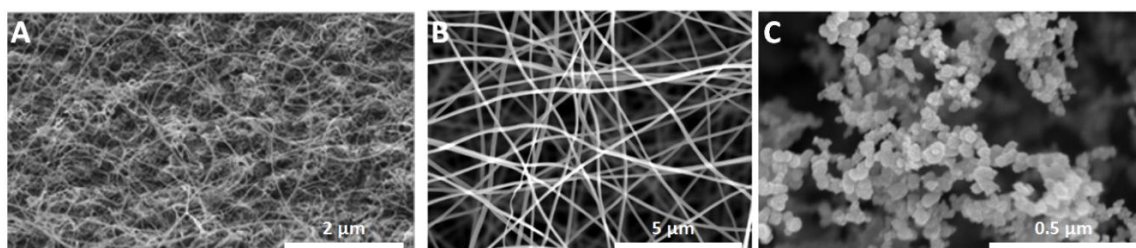


Figure 2. SEM pictures of: carbon nanotubes (CNTs) (A); carbon nanofibers (CNFs) (B); and candle soot carbon nanoparticles (CSNPs) (C). Reproduced with permission from: [55], RSC Publishing, 2015 for (A); [56], AIP Publishing, 2015 for (B); and [57], AIP Publishing, 2015 for (C).

2.2. Design and Structures

The initial investigation of LGUS transmitters is often with planar optically absorbing films, allowing relatively simple fabrication and convenient characterization. More advanced design and structures will be developed to meet a range of applications. In this subsection, a review of three types of LGUS transmitters in terms of different design and structures is presented. Figure 3 shows a schematic of fiber-optic, focused, and array transmitters.

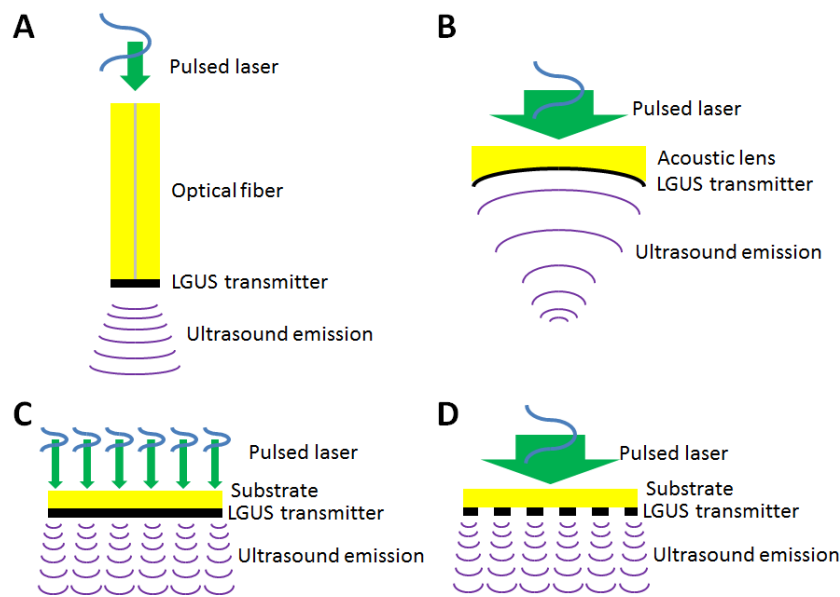


Figure 3. Schematics of: fiber-optic transmitter (A); focused transmitter (B); array transmitter with its pitch defined by spatially selective pulsed laser heating (C); and array transmitter with its pitch defined by spatially fabricated absorbers (D). Blue lines represent short laser pulses.

2.2.1. Fiber-Optic Transmitters

By implementing LGUS transmitters on optical fibers, compact devices for ultrasound generation can be realized. Such miniature transmitters can be used in highly limited space to facilitate specific applications such as IVUS imaging. The fiber-optic LGUS transmitters have suffered from their low photoacoustic conversion efficiency for quite some time. Recently, advances have been made to overcome this obstacle partly by the remarkable progress in developing highly-efficient LGUS transmitters, as detailed in Section 2.1. The photoacoustic conversion efficiency of fiber-optic LGUS transmitters is improved primarily by employing effective absorptive materials. Various applications by virtue of the unique advantages of the fiber-optic LGUS transmitters are demonstrated.

Au nanostructures are attempted for fiber-optic LGUS transmission. (i) Fabricated by a focused ion beam technique, highly absorptive Au nanopores can be patterned on the end face of an optical fiber [59]. The miniature LGUS transmitter produces ultrasound with an amplitude of 2.7 kPa and a -3 -dB bandwidth of 7 MHz. (ii) A novel Au nanocomposite, synthesized by mixing the AuNPs into PDMS following a one-pot protocol, is dipped coated on a multi-mode fiber with a core diameter of 400 μm to realize a broadband miniature fiber-optic LGUS transmitter [46]. The generated ultrasound has an amplitude of 0.64 MPa and a bandwidth of more than 20 MHz, which are significantly improved compared with the work in Reference [59]. Ultrasound imaging of a tissue sample with the resolution of 200 μm is demonstrated. (iii) Since the absorption layer on the end face of an optical fiber is essential for efficient photoacoustic conversion, numerical simulation based on finite element analysis is investigated to study the photoacoustic generation of AuNPs–PDMS nanocomposites on optical fibers [60]. (iv) The dependency of absorption efficiency of the Au nanospheres and nanorods with different organization and dimensions is simulated [45]. The results provide a useful guide to the design of fiber-optic LGUS transmitters. (v) There are many other explorations of Au nanostructures for fiber-optic LGUS transmitters such as AuNPs–polyethylenimine (PEI) nanocomposites (2.4 kPa reported) [61], AuNPs–PDMS nanocomposites (37 kPa reported) [62] and fiber sidewall ultrasound generation [47].

The carbon-based material is another promising absorber for fiber-optic LGUS transmitters. (i) Through the dissolution of CNTs in PDMS facilitated by functionalization of CNTs with oleylamine, the CNTs–PDMS nanocomposite can be dip coated on optical fibers for efficient LGUS transmission [54].

Figure 4 shows SEM pictures of fiber-optic LGUS transmitters using Au nanopores and CNTs–PDMS in References [54,59], respectively. Strong ultrasound pressure of 3.6 MPa and 4.5 MPa are measured using optical fibers with core diameters of 105 and 200 μm , respectively. The achieved pressure level is currently the best among all fiber-optic LGUS transmitters. (ii) A novel fiber-optic device based on fiber Bragg gratings is proposed to generate ultrasound at multiple, selected locations along the fiber in a scheme of light tapping where only a particular wavelength is tapped out for ultrasound generation [58]. Graphite powder and epoxy are used as LGUS transmitters in this device. The carbon-based fiber-optic LGUS transmitter typically has higher photoacoustic conversion efficiency than its metallic-based counterpart [63].

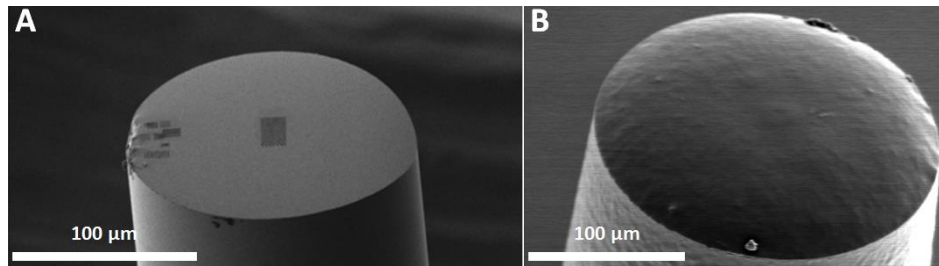


Figure 4. SEM pictures of the fiber-optic laser-generated ultrasound (LGUS) transmitters using: Au nanopores (A); and CNTs-polydimethylsiloxane (CNTs–PDMS) (B). Reproduced with permission from: [59], SPIE, 2013 for (A); and [54], AIP Publishing, 2014 for (B).

Besides broadband and efficient ultrasound generation, the fiber-optic LGUS transmitter possesses many advantages such as compact size, lightweight, ease of use, and immunity to electromagnetic interference. It may find attractive applications in all-fiber and embedded ultrasound systems for imaging and monitoring. For example, the corrosion detection is demonstrated using fiber-optic LGUS transmitters [64]. Through the characterization of the samples with different corrosion rates, effective identification of the corrosion level is achieved. The miniature device can be embedded into a structure for applications to structural health monitoring. Besides nondestructive evaluation, minimally invasive endoscopic ultrasound imaging is another promising application [65,66].

2.2.2. Focused Transmitters

High-frequency focused piezoelectric transducers are widely used for high-resolution photoacoustic and ultrasound imaging. The focused acoustic wave is achieved through the spherical surface of a focused transducer or an acoustic lens attached to a flat transducer. Borrowing from this concept, laser-generated focused acoustic wave can be realized using a focused LGUS transmitter consisting of a light-absorbing film coated on a concave spherical surface. There are several studies. (i) To develop scanning ultrasound imaging based on LGUS transmitters, an axicon transmitter is investigated to furnish high lateral resolution [67]. The achieved lateral beam size is $\sim 380 \mu\text{m}$ with non-diffracting ultrasound, also called X-waves. (ii) A concave LGUS transmitter is tested using a chromium (Cr) film with a thickness of 100 nm as the light-absorbing layer [68]. Due to high-frequency ultrasound generation by the thin film and the diffracting ultrasound by the concave lens, a high lateral beam size of $\sim 44 \mu\text{m}$ at the focus is measured. The pressure level of 20–30 kPa is achieved. (iii) When CNTs–PDMS is coated on the concave lens, an unprecedented acoustic pressure of $>50 \text{ MPa}$ is achieved by the CNTs–PDMS focused LGUS transmitter [30,69]. Figure 5 shows the experimental setup for the LGUS characterization and the fabricated lens-based LGUS transmitter. A lateral acoustic focal spot of $75 \mu\text{m}$ is obtained. Taking advantage of the remarkably high pressure in the high-frequency regime ($>15 \text{ MHz}$), micro-scale ultrasonic fragmentation and a single-cell surgery are demonstrated to show the potential for precision therapy. Moreover, the highly localized pressure and the high negative pressure facilitate the application of well-controlled bubble nucleation [70].

(iv) A new analytical model is developed to provide guidelines for the design of high-intensity and high-frequency LGUS focused transmitters [71]. (v) Focused ultrasound with complex temporal and spatial waveforms can be generated by utilizing arbitrarily shaped surfaces of polymers made by three-dimensional (3D) printing [72].

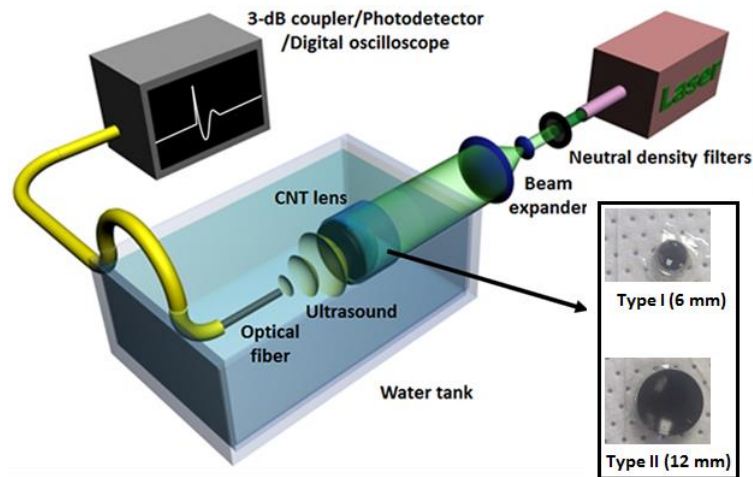


Figure 5. Measurement setup for the LGUS characterization. The laser beam is expanded and then irradiated on the CNT lens. The generated ultrasound is optically detected by scanning the fiber-optic hydrophone. Inset: two types of CNTs–PDMS focused LGUS transmitters. Reproduced with permission from [30], Nature Publishing Group, 2012.

2.2.3. Array Transmitters

LGUS is a promising approach to realize high-frequency ultrasound arrays for ultrasound beam steering and high-resolution ultrasound imaging [27,73–75]. An array element is defined by the size and location of a focused laser beam. The tiny focused spot size of the laser beam facilitates a wide-angle radiation pattern of generated ultrasound. Furthermore, a tiny array element allowing high spatial sampling is imperative for a high-frequency phased array. Several array transmitters are studied. (i) A 75-MHz, 2D phased array is demonstrated based on LGUS transmitters by mechanically scanning the focused laser beam [73]. (ii) An LGUS array transmitter using AuNPs with different diameters for different absorption wavelengths is proposed [74]. Photoacoustic excitation of an array element can be controlled by selecting different excitation wavelengths. By varying the phase delay for each laser wavelength, the ultrasound beam steering can be achieved, which eliminates the requirement for a mechanical scan. (iii) An LGUS array transmitter is created by holographic projection using a microelectromechanical systems spatial light modulator [75]. Ultrasound focusing with a focal size of 1.6 mm is achieved by projecting ring-shaped laser intensity. Focal length can be varied by changing the diameter of the ring-shaped laser excitation. Without the need of the mechanical scan, fast axial scanning microscopy is feasible.

2.3. Laser-Generated Ultrasound Applications

AOUSI is one of the most important applications of LGUS transmitters. (i) The intrinsic broad bandwidth facilitates the investigation of frequency-dependent responses in tissue, allowing the application to “virtual biopsy” [76]. (ii) Especially, when implemented based on fiber optics, AOUSI could open up a broad range of applications. A probe with a diameter of 0.84 mm for AOUSI is fabricated [77]. Axial resolution of $64\text{ }\mu\text{m}</math> and lateral resolution of $88\text{ }\mu\text{m}</math> at a depth of 3.5 mm are measured. Ex vivo vascular tissue imaging is demonstrated, as shown in Figure 6. More details about AOUSI are presented in Section 3.$$

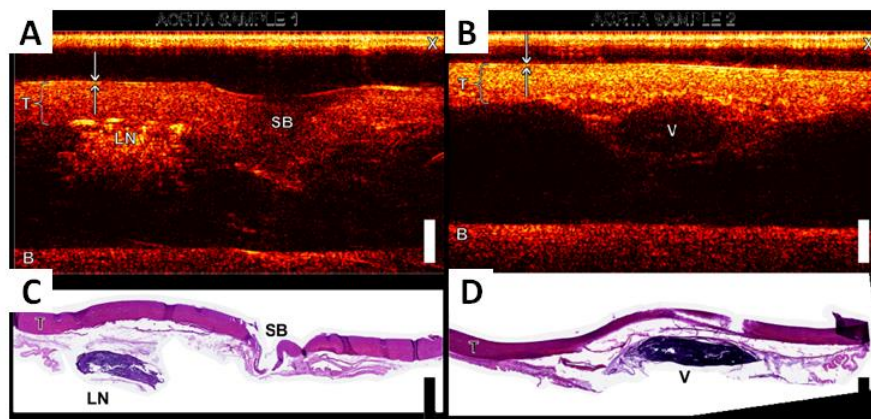


Figure 6. (A,B) All-optical ultrasound imaging (AOUSI) of swine aorta samples with a scale bar of 2 mm. B: the base of the tissue mount; LN: a lymph node; SB: a side branch; T: tunica media; V: a vessel; X: cross-talk. Arrows indicate the reflective layers, which may correspond to the intima. (C,D) The corresponding histology of aorta sections imaged in (A,B), respectively. Reproduced with permission from [77], OSA Publishing, 2015.

Besides AOUSI, the LGUS approach offers a valuable tool for nondestructive testing and biomedical applications. (i) Characterization of the resonant frequencies of a cured PDMS thin film is presented using a fiber-optic LGUS transmitter and an FP ODUS detector [78]. The received acoustic pulse is used to acquire the resonant frequencies of the PDMS thin film. (ii) A focused ultrasonic pressure pulse is used for nondestructive testing (NDT) of the surface of a sample placed in the focal zone [79,80]. Clear changes in the transient acoustic waveform are observed for the sample with cracks at the surface compared with a control sample. The approach is thus promising for nondestructive evaluation of defects. (iii) By directly irradiating the laser pulse on an absorber and analyzing the resultant photoacoustic wave, material properties can be evaluated [81]. The different states of metals can be induced using laser pulses with a wide range of intensities. By analyzing the shape and amplitude of the generated pressure, one can investigate phase transitions in metals. (iv) A fiber-optic LGUS transmitter is employed as ultrasonic tracking to accurately guide the placement of medical devices such as needles and catheters, which is critical in clinical procedures [82]. (v) The generation of controlled single microbubble is possible by relying on a highly-localized pressure by the LGUS approach [70].

3. All-Optical Ultrasound Transducers and Imaging

3.1. Development of Transducers and Imaging

Since the 1960s when the laser was discovered, optical generation and detection of ultrasound have been considered as a potential approach to overcome some limitations of conventional piezoelectric ultrasound transducers. Before the last decade, the optical-based technique was still a modern technique compared with piezoelectric transducers. It was more complex and expensive, and suffered from critical problems in relatively low efficiency in LGUS transmission and poor sensitivity in ODUS sensing. Thus, it was not widely presented in the commercial industry [83]. Piezoelectric transducers still dominated the majority of ultrasound-related applications and do the same nowadays [84,85]. In the last decade, due to the advancement of material sciences and fabrication technologies, exciting progress has been made in developing high-performance optical-based ultrasound transmitters as well as receivers.

As detailed in Section 2, LGUS transmitters have been intensely and extensively studied in the past few years. They can provide advantages such as broadband and flat frequency response, a tiny active area enabling high spatial resolution, noncontact operation facilitating applications in regions that

are difficult to reach, and good tolerance of electromagnetic interference. Driven in part by the need of novel ultrasound (and photoacoustic) imaging and detection, ODUS sensing technique has made significant progress during the last decade [32–34,37,38,86,87]. As a counterpart of LGUS transmitters, the ODUS detectors enjoy several analogous benefits, such as broadband detection, the possibility for noncontact measurement, and immunity against electromagnetic interference. Furthermore, high sensitivity can be achieved with a tiny active area, which facilitates device miniaturization.

Combining the great advantages of the LGUS transmitters and the ODUS detectors, an optical ultrasound system based on an innovative “all-optical” scheme is brought about for imaging and inspection applications. In this subsection, the recent achievement in development of AOUSTs in various aspects such as improved integration of transmitters and detectors, enhanced resolution and sensitivity, and miniaturization is described. Advanced AOUST applications that have been demonstrated very recently are also included. A summary of AOUST and AOUST developed in recent years is presented in Table A2 in Appendix.

3.1.1. Carbon-Based Transducers

CNTs–PDMS nanocomposites are efficient photoacoustic transmitters and thus are promising choices for AOUSTs. Two types of AOUSTs have been demonstrated recently. (i) A CNTs–PDMS nanocomposite film and an etalon structure consisting of $\text{SiO}_2/\text{TiO}_2$ distributed Bragg reflectors (DBRs) and an SU-8 spacer are integrated [88]. The DBR reflector allows an open spectral window for laser transmission that can be used for LGUS excitation of CNTs–PDMS nanocomposites. Compared with an Au mirror as a broadband reflector used in Reference [89], the DBR reflector circumvents the issue of little spectral window for LGUS excitation. A bandwidth of 27 MHz is obtained and a 2D transducer array is evaluated, showing the promise for high-resolution ultrasound imaging. (ii) An optical fiber with CNTs–PDMS coated on the end face of the fiber for LGUS transmission is combined with an FP etalon for ODUS sensing [90]. Strong ultrasound pressure of 21.5 MPa and a broad bandwidth of 39.8 MHz are demonstrated. AOUST of an aorta is demonstrated to show the clinical potential.

3.1.2. Fiber-Optic Transducers

The AOUST using the above-mentioned thin-film FP structure achieves high performance but is still bulky, which restricts the applications where the region of interest is difficult to access. Fiber-optic AOUSTs are explored for realizing complete miniaturized transmitting-receiving transducers. The miniaturization would facilitate the insertion of the transducer in the human body for minimally invasive procedures. Currently, fiber-optic AOUSTs are mostly constructed using two optical fibers, where one is for LGUS transmission and the other is for ODUS sensing. (i) An AOUST probe is developed with its diameter <0.84 mm and a bandwidth of ~ 20 MHz [77]. The AOUST probe and its imaging setup are shown in Figure 7. It consists of an LGUS transmitter using a CNTs–PDMS nanocomposite coating on the end face of an optical fiber and an FP ODUS receiver on that of an adjacent optical fiber. The generation and detection fibers are within tubular metal housing. The probe is mechanically scanned to form a virtual array for synthetic aperture [91]. The lateral and axial resolutions are measured as 88 and 64 μm , respectively, at a depth of 3.5 mm. (ii) An LGUS array transmitter is implemented using AuNPs with different sizes on the end face of an optical fiber [74]. A fiber-optic FP cavity is fabricated on the same fiber as the ODUS detector. One unique property of AuNPs is that their maximum absorption wavelength varies with the diameters of AuNPs. Laser with different wavelengths can be chosen to excite AuNPs with corresponding sizes at specific locations. Such excitation scheme facilitates the realization of phased array technique and ultrasound beam steering. It is not necessary to perform a mechanical scan for 3D imaging. A bundle of hollow optical fibers may also be considered as another approach to construct an LGUS array transmitter [92]. (iii) Through employing an acoustic lens for geometrical focusing, a fiber-optic LGUS transmitter that can produce a collimated ultrasound beam is demonstrated [93]. When the transmitter is integrated with a fiber-optic ODUS detector, an AOUST probe can be constructed. Since the beam is well

collimated, pulse-echo ultrasound imaging can be acquired by scanning the probe without the need for image reconstruction. (iv) Another work shows that the AOUST probe can be fabricated based on a micro-opto-mechanical-system (MOMS) process [94].

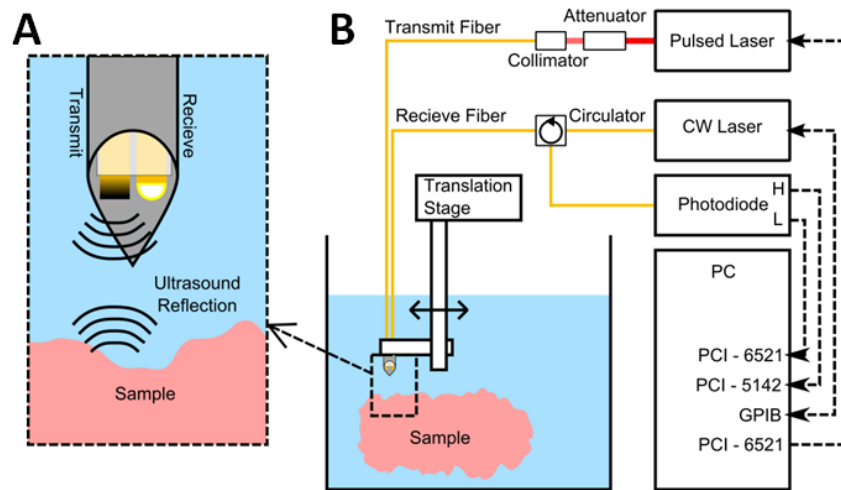


Figure 7. (A) The fiber-optic all-optical ultrasound transducer (AOUST) consisting of an optical fiber with a CNTs–PDMS nanocomposite coating for LGUS transmission and an adjacent fiber with an Fabry-Perot (FP) etalon for optical detection of ultrasound (ODUS) sensing. Tubular metal housing is also shown. (B) The imaging system for the AOUST probe. CW: continuous wave; GPIB: general purpose interface bus; PCI: peripheral component interconnect. Reproduced with permission from [77], OSA Publishing, 2015.

3.1.3. Performance Enhancement

Suitable integration of LGUS transmitters and ODUS detectors into an AOUST is not only for convenient operation, but also for keeping the superiority of high-frequency and broadband operation. The ultrasound transmission and detection of the piezoelectric transducer is naturally well coordinated because the acoustic wave is generated and detected through the same piezoelectric material. Unlike the piezoelectric transducer, the ultrasound transmission and detection based on the optical method should be well organized deliberately. Otherwise, there could be some issues such as a long propagation distance and/or a large incident angle from the ultrasound generation to detection, leading to attenuation and distortion of measured acoustic signals, especially for high-frequency components. In addition, one may suffer from the problem of demanding and time-consuming alignment in scanning microscopy and the difficulty of arranging the set up in a reflection-mode operation for convenient applications. Several decent approaches of integration are demonstrated.

(i) A broadband AOUST consists of a 2D Au nanostructure on a glass substrate, followed by a PDMS layer and a Au layer [28,29]. The Au nanostructure is for LGUS transmission, while the Au–PDMS–Au structure is used as an FP etalon for ODUS sensing. Pulse-echo ultrasound with a broad bandwidth of 57 MHz is demonstrated. High-frequency ultrasound arrays are also proposed through directing both the ultrasound generation and detection laser beams into an array of focused spots on the device surface. Another similar work employs black PDMS for LGUS transmission [89].

(ii) An improved design using a polyimide-etalon thin film structure is demonstrated [95,96]. As for the AOUST using 2D Au nanostructure [28,29], the excitation laser intensity is partly absorbed by the Au nanostructure and partly absorbed by the FP etalon, which results in damage to the FP receiver and is not suitable for long-term use. As for the one using black PDMS [89], the configuration prohibits transmitter and receiver elements from being in the same location, which is undesired for imaging purposes. The polyimide-etalon AOUST overcomes the above obstacles by utilizing the unique characteristics of the polyimide that is highly absorptive in a narrow spectrum, ultraviolet

range, for LGUS transmission and highly transparent to wavelengths, near-infrared range, for FP sensing. Thus, high lateral resolutions of 70 and 114 μm at depths of 2.4 and 5.8 mm, respectively, with an average axial resolution of 35 μm are obtained.

(iii) An intriguing excitation method is proposed for AOUSTs for resolution and efficiency enhancement [97]. Pulsed laser excitation is commonly used to produce ultrasound with broad bandwidth. Energy loss could happen in certain frequency bands due to acoustic attenuation within tissues, nonuniform acoustic power spectra in generation or nonuniform acoustic sensing spectra in detection, leading to reduced system efficiency and bandwidth. By using an optical modulation for ultrasound excitation, the bandwidth can be constrained to those frequencies determined by the process of all-optical ultrasound transduction. Through pulse-echo imaging experiment, a linear chirp excitation presents similar axial resolution and signal-to-noise ratios (SNRs) compared with conventional pulsed laser excitation. Furthermore, a nonlinear chirp excitation, where the nonlinearity should be determined based on the spectral sensitivity of the system, can be used to increase the bandwidth and consequently the axial resolution, at the expense of a lower SNR.

3.1.4. Multi-Modality Imaging

By integrating AOUSI with all-optical photoacoustic imaging (AOPAI) [98,99], complementary information originated from contrasts of acoustic impedance and light absorption can be provided. Owing to the same signal form acquired by ultrasound and photoacoustic (US/PA) imaging, acoustic waves for each modality can be captured using one ODUS detector. Thus, the advantages such as high spatial resolution and easy miniaturization existing in AOUSI can be shared with AOPAI. There are several US/PA dual-modality imaging systems developed based on an all-optical approach. (i) A scanhead consisting of an optical fiber with an axicon tip for LGUS and photoacoustic excitation for AOUSI and AOPAI, respectively, and an optical microring resonator for acoustic detection of the two imaging modes is demonstrated [100]. A single laser pulse is used to generate both US/PA signals, and thus, the information for both images is received simultaneously. (ii) The approach of simultaneous US/PA excitation using a single laser pulse is employed in another all-optical US/PA imaging setup, where an optical integrating detector is used for acquiring signals for US/PA imaging [101]. (iii) Instead of using a single laser pulse for US/PA excitation, all-optical US/PA scanhead is built using a dichroic filter to select the laser wavelengths for switching between the two imaging modes [102], where the microring resonator is used for signal detection. Figure 8 shows the mechanisms for US/PA imaging.

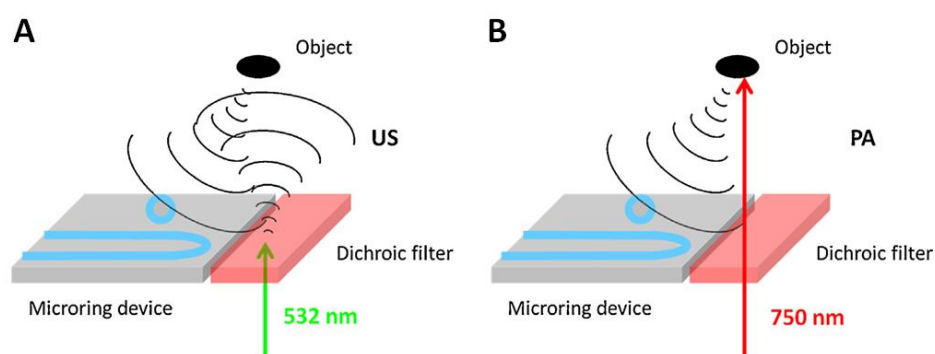


Figure 8. (A) Schematic of ultrasound imaging where the 532-nm laser is absorbed by the dichroic filter. (B) Schematic of photoacoustic imaging where the 750-nm laser passes through the filter for photoacoustic excitation. Reproduced with permission from [102], Elsevier GmbH, 2014.

3.2. Imaging Applications

As the promising development of AOUSTs, advanced applications by AOUSI are of particular interest. Several biomedical imaging applications are demonstrated. (i) The high frequency and

broad bandwidth associated with the all-optical approach can potentially be used for virtual biopsy of biological tissue [94]. (ii) Vascular tissue imaging is studied by an AOUST probe [77]. The ultrasound images of vascular tissues from swine aorta show good correspondence with histological images. (iii) A miniature needle probe for AOUSI is developed for the applications in guiding interventional pain management procedures [103]. The probe is able to provide real-time M-mode images. (iv) An ultra-high resolution AOUSI system is built to investigate cell mechanics [104]. The information of mechanical properties with a sub-cell resolution is significantly useful to study fundamental biological processes and disease conditions. The system operates in the 10 to 100 GHz range and thus provides a sub-cell resolution of 10 nm. Figure 9 shows AOUSI cell images of the nuclear region and lamellipodium and their white-light images for comparison. With such ultra-high resolution, details of cells can be resolved. (v) A miniature side-looking AOUST probe is developed for IVUS imaging [105]. The axial resolution of 70 μm and the imaging depth in tissue greater than 1 cm are achieved. Ex vivo imaging of tissues including swine tissue and diseased human tissue is demonstrated, showing the potential of this probe for IVUS applications.

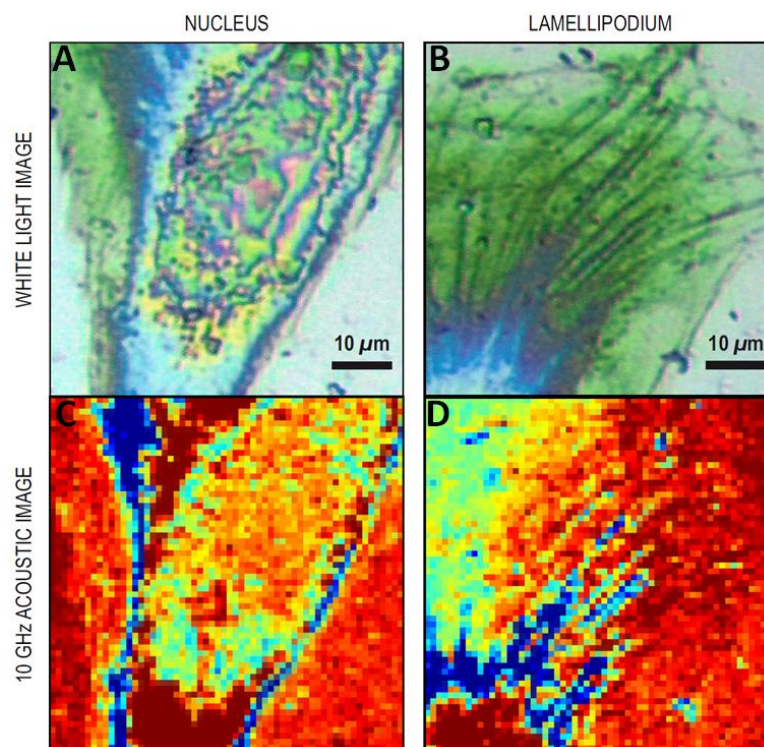


Figure 9. AOUSI cell images (taken at 10 GHz) of: the nuclear region (C); and lamellipodium (D). The upper row shows white-light images of: the nuclear region (A); and lamellipodium (B) for comparison. The scale bar of 10 μm applies to all images. The contour of the cell, the structure of the nucleus and the fine details of the fibrillar lamellipodium are clearly observed by the very high acoustic contrast. Reproduced with permission from [104], Nature Publishing Group, 2015.

4. Summary and Prospects

In this review, the recent advances that have been made for LGUS transmitters are presented. Table A1 gives an overview of various developed LGUS transmitters. Table A2 provides the development of AOUSTs and their AOUSI applications. The review shows that the performance of LGUS transmitters has been constantly improved in recent years by advances in material science and fabrication technology. From the engineering viewpoint, the performance of LGUS transmitters has been significantly improved in a range of aspects, including transmitting efficiency, imaging resolution, size miniaturization, beam focusing and shaping, and functionality. From the application

viewpoint, LGUS technique has been demonstrated for its potential in a number of applications including biomedical imaging, therapeutic ultrasound, and non-destructive evaluation. The LGUS platform possesses several advantages that can overcome limitations of conventional piezoelectric ultrasound method. (i) Through thermoelastic approach, the LGUS transmitters can generate a broadband ultrasound (from tens of MHz to even hundreds of GHz) provided that a short laser pulse is used to irradiate on an absorptive thin film. This is because the mechanism is based on photoacoustic effect, instead of the resonant characteristics used in piezoelectric transducers. In addition, flat spectral response can be intrinsically achieved. (ii) Imaging with high spatial resolution can be achieved. For ultrasound imaging, high resolution can be provided by either focusing acoustic waves to a diffraction-limited spot size or generating ultrasound in small pitches for phased array implementation. Both approaches can be realized by the LGUS method. Together with its capability to generate ultrasound with high frequency and broad bandwidth, the LGUS platform can provide high resolutions in both the lateral and axial directions. (iii) When combined with a noncontact ODUS sensing technique, LGUS technique provides a completely remote system that can be applied to harsh regions that are difficult to access, such as high pressure and high temperature [106], corrosive, and radioactive environments. Since it is a noncontact approach, it will not interfere with the sample being evaluated. (iv) LGUS technique also offers high tolerance to electromagnetic interference. (v) The fast development in LGUS technology has, in turn, triggered growing interest in constructing AOUSTs and their imaging applications to biomedicine. AOUSTs have unique advantages in certain aspects over traditional piezoelectric ultrasound imaging. It seems to be observed that the growing interest and development speed of these techniques in medical imaging are faster than those in industrial applications.

Effective and broadband LGUS transmitters should possess high conversion efficiency of radiation energy to heat, large coefficients of thermal expansion, and fast heat diffusion to the surroundings. Deduced by the above review, several principles can be followed when choosing suitable LGUS transmitters. (i) As for the absorbers, metallic or carbon-based materials should have low specific heat capacity for high light-to-heat conversion efficiency. (ii) As for the surrounding medium, materials such as PDMS with large coefficients of thermal expansion are desired for high heat-to-ultrasound conversion efficiency. (iii) The size of absorptive materials has a significant impact on their heat transition to the surrounding medium. The nanoscale dimension of absorbers allows short thermal diffusion time, which is essential for high-frequency ultrasound generation. In addition to the size, high thermal conductivity of the absorber and high thermal diffusivity of the surrounding medium are helpful for optimization of fast heat transition. (iv) LGUS transmitters are better to be made in the form of a film on a transparent substrate or a solid freestanding film, which facilitates laser illumination and their use in water or liquid environment. (v) A tradeoff between the light absorption and film thickness for optimization between the amplitude and bandwidth of generated ultrasound should be considered in designing LGUS transmitters. (vi) For AOUSTs, suitable and elegant integration of LGUS transmitters and ODUS detectors are of great significance in imaging performance and size miniaturization. Despite intense investigation in recent years, LGUS technology still has a lot of room for improvement. The following future directions are of practical significance. (i) The nanocomposites capable of highly-efficient photoacoustic conversion hold great promise for high-amplitude LGUS transmission. Further optimization of these nanocomposites is still a lack of LGUS research. The optimization includes an optimal density or ratio of the absorber in the whole composite, suitable arrangement of the absorber and the surrounding material, enhancement of optical extinction in thin-film transmitters, and robustness against high optical fluence. Such optimization can potentially be used for advanced diagnostic and therapeutic applications. (ii) The future research of fiber-optic LGUS transmitters for interventional imaging and therapy should emphasize their biocompatibility and safety. The toxicity of nanocomposites used as part of medical devices is not fully tested yet. How to reduce side effects and how to ensure a safe delivery of strong laser pulses are key issues in this research. The power of ultrasound should be below the threshold pain level

(<1.5 W/cm²) [107], and the fluence of any single laser pulse on the skin surface should follow the ANSI standard (<20 mJ/cm²). (iii) Multi-modality imaging provides complementary information. Besides AOUSI, photoacoustic imaging and other imaging modes, if integrated, will notably improve the acquired medical information about functional physiology and pathology. In addition, development of multi-modality endoscopy is promising by taking advantage of recent progress in optical endoscopic probes [108,109]. AOUST may share several components of the optical probes, which facilitates the incorporation of ultrasound modality. (iv) The application of LGUS transmitters for real-time ultrasound imaging is rarely investigated. Development of an LGUS-based high-speed imaging system that meets the needs of modern medicine is a valuable research direction for the future. Array implementation of LGUS transmitters, as well as ultrasound receivers, can be one approach to realize real-time ultrasound imaging. (v) The majority of current research focus of LGUS technology still lies in basic research. More clinical and industrial tests should be conducted for its prevalence.

LGUS transmitters and their use for AOUSI could provide groundbreaking opportunities for high-resolution imaging and detection, precise localization, image-guided surgery and therapy, interventional procedures, and remote sensing. With advances in LGUS technology, LGUS transmitters and AOUSI systems will continue to improve on their performance and functionality in the coming years, and thus, advanced applications such as high-resolution endoscopic diagnosis and real-time non-destructive assessment becomes possible. Further research on LGUS is of great importance to transform research studies into practical or clinical prevalence.

Acknowledgments: This work was supported by the National Natural Science Foundation of China (No. 61405112), the National High Technology Research and Development Program of China (863 Program) (No. 2015AA020944), and the Shanghai Science and Technology Committee (No. 15140901400).

Author Contributions: Sung-Liang Chen proposed this subject, collected previous works and wrote the paper.

Conflicts of Interest: The author declares no conflict of interest.

Appendix

Tables A1 and A2 summarize the characteristics of LGUS transmitters and AOUSTs with their applications to AOUSI, respectively.

Table A1. Summary of the characteristics of laser-generated ultrasound transmitters, AuNPs: gold nanoparticles; CB: carbon black; CNFs: carbon nanofibers; CNTs: carbon nanotubes; CSNPs: candle soot carbon nanoparticles; NDT: nondestructive testing; PDMS: polydimethylsiloxane; rGO: reduced graphene oxide.

Absorptive Material-Elastomer	Design and Structure	Specification	Peak Pressure (MPa)	Laser Density (mJ/cm ²)	Band-Width (MHz)	Application	Reference
AuNPs-PDMS	Planar	-	0.0027	~20	-	-	[43]
AuNPs-PDMS	Planar	-	0.19	13	3.1	-	[39]
AuNPs-PDMS	Fiber	Core size: 400 μm	0.0075	-	-	-	[60]
AuNPs-PDMS	Fiber	Core size: 400 μm	0.037	126	2.1	-	[62]
AuNPs-PDMS	Fiber	Core size: 400 μm	0.64	8.75	>20	Tissue imaging	[46]
AuNPs	Fiber	-	0.0024	~4200	-	-	[61]
AuNPs	Fiber	Array element ¹	0.0016	1770	-	-	[74]
Au nanopores	Fiber	Core size: 62.5 μm	0.0027	~100	7	-	[59]
Au	Planar	-	0.24	23	78	-	[40]
Al with rGO	Planar	-	~9	56	-	-	[49]
Al	Array	Array element ²	-	-	-	-	[75]
Steel	Focused	Aperture: 28 mm	1	~10	-	NDT of cracks	[79]
Cr	Focused	Aperture: 6.35 mm	0.02–0.03	~0.5	-	-	[68]
CNFs-PDMS	Planar	-	12	3.7	8	-	[56]
CSNPs-PDMS	Planar	-	4.8	3.6	21	-	[57]
CNTs-PDMS	Fiber	Core size: 200 μm	4.5	36	15	-	[54]
CNTs-PDMS	Fiber	Core size: 200 μm	4	96	20	-	[77]
CNTs-PDMS	Focused	Aperture: 6 mm	57	260–270	-	High-precision therapy	[30]
CNTs-PDMS	Focused	Aperture: 15 mm	30	20	-	-	[72]
CB-PDMS	Planar	-	0.8	~10,000	-	-	[52]
CB-PDMS	Array	Array element ³	-	-	~100	-	[27]
CB-PDMS	Array	Array element ⁴	-	-	~100	-	[73]
Graphite powder	Fiber	Core size: 600 μm	0.15	~3.5	50	-	[76]
Black acrylic dye	Focused	-	~0.02	-	-	-	[67]

¹ Element defined by different sizes of AuNPs; ² element defined by micro-mirror spatial light modulator; ³ element defined by optical focused spot (15 μm). ⁴ Element defined by optical focused spot (5 μm).

Table A2. Summary of all-optical ultrasound transducers and imaging, AOUSI: all-optical ultrasound imaging; FP: Fabry–Perot; IVUS: intravascular ultrasound; US/PA: ultrasound and photoacoustic.

Laser-Generated Ultrasound			Optical Ultrasound Detection	Performance: Bandwidth (MHz); Lateral Resolution (μm); Axial Resolution (μm)	Imaging or Application	Reference
Absorptive Material-Elastomer	Design and Structure	Specification				
AuNPs	Planar	-	Thin-film FP etalon	57; 38; 19	-	[28,29]
CB–PDMS	Planar	-	Thin-film FP etalon	40; NA; NA	-	[89]
CNTs–PDMS	Planar	-	Thin-film FP etalon	27; NA; NA	-	[88]
Polyimide	Planar	-	Thin-film FP etalon	29; 71; 35	-	[95]
Polyimide	Planar	-	Thin-film FP etalon	~48; 70; 35	-	[96]
Silicon	Planar	-	Microring resonator	28; 305; 169	US/PA dual modality	[100]
Dichroic filter	Planar	-	Microring resonator	~17; 2.52° ¹ ; 125	US/PA dual modality	[102]
Ti	Planar	-	Pump-probe detection	~10 ⁵ ; 2; NA	Cell mechanics	[104]
CNTs–PDMS	Fiber	Core size: 200 μm ²	Fiber FP etalon	~20; 88; 64	AOUSI of swine aorta	[77]
CNTs–PDMS	Fiber	-	Thin-film FP etalon	~40; NA; NA	AOUSI of swine aorta	[90]
CNTs–PDMS	Fiber	Core size: 200 μm	Fiber FP etalon	NA	Real-time guidance	[103]
CNTs–PDMS	Fiber	-	Fiber FP etalon	NA; NA; 60	IVUS	[105]
Carbon	Fiber	-	Fiber FP etalon	40–50; NA; NA	-	[94]
AuNPs	Fiber, array	-	Fiber FP etalon	NA	-	[74]
CB	Fiber, focused	Lens aperture: 2 mm	Fiber FP etalon	-	AOUSI of aorta	[93]
Cr	Focused	Cylindrical focus	Integrating detector	~18; ~60 ³	US/PA dual modality	[101]

¹ Lateral resolution is in the unit of degree; ² Overall diameter of the AOUST probe is <0.84 mm; ³ In-plane resolution.

References

1. *Learning Ultrasound Imaging*, 1st ed.; del Cura, J.L.; Seguí, P.; Nicolau, C., Eds.; Springer: Berlin/Heidelberg, Germany, 2012.
2. Das, A.; Sivak, M.V.; Chak, A.; Wong, R.C.; Westphal, V.; Rollins, A.M.; Willis, J.; Isenberg, G.; Izatt, J.A. High-resolution endoscopic imaging of the GI tract: A comparative study of optical coherence tomography versus high-frequency catheter probe EUS. *Gastrointest. Endosc.* **2001**, *54*, 219–224. [[CrossRef](#)] [[PubMed](#)]
3. Fledelius, H.C. Ultrasound in ophthalmology. *Ultrasound Med. Biol.* **1997**, *23*, 365–375. [[CrossRef](#)]
4. Nair, A.; Kuban, B.D.; Tuzcu, E.M.; Schoenhagen, P.; Nissen, S.E.; Vince, D.G. Coronary plaque classification with intravascular ultrasound radiofrequency data analysis. *Circulation* **2002**, *106*, 2200–2206. [[CrossRef](#)] [[PubMed](#)]
5. Schmid-Wendtner, M.H.; Burgdorf, W. Ultrasound scanning in dermatology. *Arch. Dermatol.* **2005**, *141*, 217–224. [[CrossRef](#)] [[PubMed](#)]
6. Van Wijk, D.F.; Strang, A.C.; Duivenvoorden, R.; Enklaar, D.J.; van der Geest, R.J.; Kastelein, J.J.P.; de Groot, E.; Stroes, E.S.G.; Nederveen, A.J. Increasing spatial resolution of 3T MRI scanning improves reproducibility of carotid arterial wall dimension measurements. *Magn. Reson. Mater. Phys.* **2014**, *27*, 219–226. [[CrossRef](#)] [[PubMed](#)]
7. Zhao, Y.; Brun, E.; Coan, P.; Huang, Z.; Sztrókayd, A.; Diemoz, P.C.; Liebhardt, S.; Mitton, A.; Gasilovc, S.; Miaoa, J.; et al. High-resolution, low-dose phase contrast X-ray tomography for 3D diagnosis of human breast cancers. *Proc. Natl. Acad. Sci. USA* **2012**, *109*, 18290–18294. [[CrossRef](#)] [[PubMed](#)]
8. Wang, L.V.; Wu, H.I. *Biomedical Optics: Principles and Imaging*, 1st ed.; John Wiley & Sons, Inc.: Hoboken, NJ, USA, 2007.
9. Beaurepaire, E.; Boccaro, A.C.; Lebec, M.; Blanchot, L.; Saint-Jalmes, H. Full-field optical coherence microscopy. *Opt. Lett.* **1998**, *23*, 244–246. [[CrossRef](#)] [[PubMed](#)]
10. Wang, L.V. Multiscale photoacoustic microscopy and computed tomography. *Nat. Photonics* **2009**, *3*, 503–509. [[CrossRef](#)] [[PubMed](#)]
11. Wang, L.V.; Hu, S. Photoacoustic tomography: In vivo imaging from organelles to organs. *Science* **2012**, *335*, 1458–1462. [[CrossRef](#)] [[PubMed](#)]
12. Bossy, E.; Gigan, S. Photoacoustics with coherent light. *Photoacoustics* **2016**, *4*, 22–35. [[CrossRef](#)] [[PubMed](#)]
13. Tanter, M.; Fink, M. Ultrafast imaging in biomedical ultrasound. *IEEE Trans. Ultrason. Ferroelectr. Freq. Control* **2014**, *61*, 102–119. [[CrossRef](#)] [[PubMed](#)]
14. Correia, M.; Provost, J.; Tanter, M.; Pernot, M. 4D ultrafast ultrasound flow imaging: In vivo quantification of arterial volumetric flow rate in a single heartbeat. *Phys. Med. Biol.* **2016**, *61*, L48–L61. [[CrossRef](#)] [[PubMed](#)]
15. Dubinsky, T.J.; Cuevas, C.; Dighe, M.K.; Kolokythas, O.; Hwang, J.H. High-intensity focused ultrasound: Current potential and oncologic applications. *AJR Am. J. Roentgenol.* **2008**, *190*, 191–199. [[CrossRef](#)] [[PubMed](#)]
16. Larrat, B.; Pernot, M.; Aubry, J.F.; Dervishi, E.; Sinkus, R.; Seilhean, D.; Marie, Y.; Boch, A.L.; Fink, M.; Tanter, M. MR-guided transcranial brain HIFU in small animal models. *Phys. Med. Biol.* **2010**, *55*, 365–388. [[CrossRef](#)] [[PubMed](#)]
17. Liu, R.; Kim, H.H.; Cannata, J.M.; Chen, G.S.; Shung, K.K. 10F-4 Self-focused 1–3 composite LiNbO₃ single element transducers for high frequency HIFU applications. In Proceedings of the 2007 IEEE International Ultrasonics Symposium, New York, NY, USA, 28–31 October 2007; pp. 949–952.
18. Ladabaum, I.; Jin, X.; Soh, H.Y.; Atalar, A.; Khuri-Yakub, B.T. Surface micromachined capacitive ultrasonic transducers. *IEEE Trans. Ultrason. Ferroelectr. Freq. Control* **1998**, *45*, 678–690. [[CrossRef](#)] [[PubMed](#)]
19. Eccardt, P.C.; Niederer, K. Micromachined ultrasound transducers with improved coupling factors from a CMOS compatible process. *Ultrasonics* **2000**, *38*, 774–780. [[CrossRef](#)]
20. Park, K.K.; Oralkan, O.; Khuri-Yakub, B.T. A comparison between conventional and collapse-mode capacitive micromachined ultrasonic transducers in 10-MHz 1-D arrays. *IEEE Trans. Ultrason. Ferroelectr. Freq. Control* **2013**, *60*, 1245–1255. [[CrossRef](#)] [[PubMed](#)]
21. Gurun, G.; Tekes, C.; Zahorian, J.; Xu, T.; Satir, S.; Karaman, M.; Hasler, J.; Degertekin, F.L. Single-chip CMUT-on-CMOS front-end system for real-time volumetric IVUS and ICE imaging. *IEEE Trans. Ultrason. Ferroelectr. Freq. Control* **2014**, *61*, 239–250. [[CrossRef](#)] [[PubMed](#)]
22. Hou, Y. Broadband All-Optical Ultrasound Transducers for High-Resolution Ultrasound Imaging. Ph.D. Thesis, University of Michigan, Ann Arbor, MI, USA, 2008.

23. Scruby, C.B.; Drain, L.E. *Laser Ultrasonics Techniques and Applications*; CRC Press: Boca Raton, FL, USA, 1990.
24. Gusev, V.E.; Karabutov, A.A. *Laser Optoacoustics*; American Institute of Physics: College Park, MD, USA, 1993.
25. Davies, S.J.; Edwards, C.; Taylor, G.S.; Palmer, S.B. Laser-generated ultrasound: Its properties, mechanisms and multifarious applications. *J. Phys. D* **1993**, *26*, 329–348. [[CrossRef](#)]
26. Wang, L.V. Tutorial on photoacoustic microscopy and computed tomography. *IEEE J. Sel. Top. Quantum Electron.* **2008**, *14*, 171–179. [[CrossRef](#)]
27. Buma, T.; Spisar, M.; O'Donnell, M. High-frequency ultrasound array element using thermoelastic expansion in an elastomeric film. *Appl. Phys. Lett.* **2001**, *79*, 548–550. [[CrossRef](#)]
28. Hou, Y.; Kim, J.S.; Ashkenazi, S.; Huang, S.W.; Guo, L.J.; O'Donnell, M. Broadband all-optical ultrasound transducers. *Appl. Phys. Lett.* **2007**, *91*, 073507. [[CrossRef](#)]
29. Hou, Y.; Kim, J.S.; Huang, S.W.; Ashkenazi, S.; Guo, L.J.; O'Donnell, M. Characterization of a broadband all-optical ultrasound transducer from optical and acoustical properties to imaging. *IEEE Trans. Ultrason. Ferroelectr. Freq. Control* **2008**, *55*, 1867–1877. [[PubMed](#)]
30. Baac, H.W.; Ok, J.G.; Maxwell, A.; Lee, K.T.; Chen, Y.C.; Hart, A.J.; Xu, X.; Yoon, E.; Guo, L.J. Carbon-nanotube optoacoustic lens for focused ultrasound generation and high-precision targeted therapy. *Sci. Rep.* **2012**, *2*, 989. [[CrossRef](#)] [[PubMed](#)]
31. Lee, T.; Baac, H.W.; Ok, J.G.; Youn, H.S.; Guo, L.J. Nozzle-free liquid microjetting via homogeneous bubble nucleation. *Phys. Rev. Appl.* **2015**, *3*, 044007. [[CrossRef](#)]
32. Zhang, C.; Ling, T.; Chen, S.L.; Guo, L.J. Ultrabroad bandwidth and highly sensitive optical ultrasonic detector for photoacoustic imaging. *ACS Photonics* **2014**, *1*, 1093–1098. [[CrossRef](#)]
33. Hamilton, J.D.; Buma, T.; Spisar, M.; O'Donnell, M. High frequency optoacoustic arrays using etalon detection. *IEEE Trans. Ultrason. Ferroelectr. Freq. Control* **2000**, *47*, 160–169. [[CrossRef](#)] [[PubMed](#)]
34. Paltauf, G.; Nuster, R.; Haltmeier, M.; Burgholzer, P. Photoacoustic tomography using a Mach-Zehnder interferometer as an acoustic line detector. *Appl. Opt.* **2007**, *46*, 3352–3358. [[CrossRef](#)] [[PubMed](#)]
35. Xie, Z.; Chen, S.L.; Ling, T.; Guo, L.J.; Carson, P.L.; Wang, X. Pure optical photoacoustic microscopy. *Opt. Express* **2011**, *19*, 9027–9034. [[CrossRef](#)] [[PubMed](#)]
36. Hou, Y.; Huang, S.W.; Ashkenazi, S.; Witte, R.; O'Donnell, M. Thin polymer etalon arrays for high-resolution photoacoustic imaging. *J. Biomed. Opt.* **2008**, *13*, 064033. [[CrossRef](#)] [[PubMed](#)]
37. Ling, T.; Chen, S.L.; Guo, L.J. High-sensitivity and wide-directivity ultrasound detection using high Q polymer micro-ring resonators. *Appl. Phys. Lett.* **2011**, *98*, 204103. [[CrossRef](#)] [[PubMed](#)]
38. Zhang, C.; Chen, S.L.; Ling, T.; Guo, L.J. Review of imprinted polymer microring as ultrasound detector: Design, fabrication, and characterization. *IEEE Sens. J.* **2015**, *15*, 3241–3248. [[CrossRef](#)]
39. Wu, N.; Tian, Y.; Zou, X.; Silva, V.; Chery, A.; Wang, X. High-efficiency optical ultrasound generation using one-pot synthesized polydimethylsiloxane-gold nanoparticle nanocomposite. *J. Opt. Soc. Am. B* **2012**, *29*, 2016–2020. [[CrossRef](#)]
40. Guo, Y.; Baac, H.W.; Chen, S.L.; Norris, T.B.; Guo, L.J. Broad-band high-efficiency optoacoustic generation using a novel photonic crystal-metallic structure. *Proc. SPIE* **2011**, 7899, 78992C–78992C-8.
41. White, R.M. Generation of elastic waves by transient surface heating. *J. Appl. Phys.* **1963**, *34*, 3559–3567. [[CrossRef](#)]
42. Kang, S.; Yoon, Y.; Kim, J.; Kim, W. Thermoelastic response of thin metal films and their adjacent materials. *Appl. Phys. Lett.* **2013**, *102*, 021908. [[CrossRef](#)]
43. Hou, Y.; Kim, J.S.; Ashkenazi, S.; O'Donnell, M.; Guo, L.J. Optical generation of high frequency ultrasound using two-dimensional gold nanostructure. *Appl. Phys. Lett.* **2006**, *89*, 093901. [[CrossRef](#)]
44. Sassaroli, E.; Li, K.C.P.; O'Neill, B.E. Numerical investigation of heating of a gold nanoparticle and the surrounding microenvironment by nanosecond laser pulses for nanomedicine applications. *Phys. Med. Biol.* **2009**, *54*, 5541–5560. [[CrossRef](#)] [[PubMed](#)]
45. Tian, Y.; Jaradat, H.; Wu, N.; Zou, X.; Zhang, Y.; Liu, Y.; Akyurtlu, A.; Cao, C.; Wang, X. Numerical simulation of gold nanostructure absorption efficiency for fiber-optic photoacoustic generation. *Prog. Electromagn. Res. Lett.* **2013**, *42*, 209–223. [[CrossRef](#)]
46. Zou, X.; Wu, N.; Tian, Y.; Wang, X. Broadband miniature fiber optic ultrasound generator. *Opt. Express* **2014**, *22*, 18119–18127. [[CrossRef](#)] [[PubMed](#)]
47. Zhou, J.; Wu, N.; Bi, S.; Wang, X. Ultrasound generation from an optical fiber sidewall. *Proc. SPIE* **2016**, 98031U. [[CrossRef](#)]

48. Soltani, P.; Akbareian, N. Finite element simulation of laser generated ultrasound waves in aluminum plates. *Lat. Am. J. Solids Struct.* **2014**, *11*, 1761–1776. [[CrossRef](#)]
49. Lee, S.H.; Park, M.A.; Yoh, J.J.; Song, H.; Jang, E.Y.; Kim, Y.H.; Kang, S.; Yoon, Y.S. Reduced graphene oxide coated thin aluminum film as an optoacoustic transmitter for high pressure and high frequency ultrasound generation. *Appl. Phys. Lett.* **2012**, *101*, 241909.
50. Karabutov, A.A.; Kaptilniy, A.G.; Ivochkin, A.Y.; Ksenofontov, D.M.; Trofimov, A.D. Optoacoustic study of laser-induced near-critical states of thin aluminum films. *Moscow Univ. Phys.* **2013**, *68*, 383–386. [[CrossRef](#)]
51. Yoo, G.; Park, Y.; Sang, P.; Baac, H.W.; Heo, J. High-frequency optoacoustic transmitter based on nanostructured germanium via metal-assisted chemical etching. *Opt. Mater. Express* **2016**, *6*, 2567–2572. [[CrossRef](#)]
52. Hou, Y.; Ashkenazi, S.; Huang, S.W.; O'Donnell, M. Improvements in optical generation of high-frequency ultrasound. *IEEE Trans. Ultrason. Ferroelectr. Freq. Control* **2007**, *54*, 682–686. [[CrossRef](#)] [[PubMed](#)]
53. Baac, H.W.; Ok, J.G.; Park, H.J.; Ling, T.; Chen, S.L.; Hart, A.J.; Guo, L.J. Carbon nanotube composite optoacoustic transmitters for strong and high frequency ultrasound generation. *Appl. Phys. Lett.* **2010**, *97*, 234104. [[CrossRef](#)] [[PubMed](#)]
54. Colchester, R.J.; Mosse, C.A.; Bhachu, D.S.; Bear, J.C.; Carmalt, C.J.; Parkin, I.P.; Treeby, B.E.; Papakonstantinou, I.; Desjardins, A.E. Laser-generated ultrasound with optical fibres using functionalised carbon nanotube composite coatings. *Appl. Phys. Lett.* **2014**, *104*, 173502. [[CrossRef](#)]
55. Baac, H.W.; Ok, J.G.; Lee, T.; Guo, L.J. Nano-structural characteristics of carbon nanotube–polymer composite films for high-amplitude optoacoustic generation. *Nanoscale* **2015**, *7*, 14460–14468. [[CrossRef](#)] [[PubMed](#)]
56. Hsieh, B.Y.; Kim, J.; Zhu, J.; Li, S.; Zhang, X.; Jiang, X. A laser ultrasound transducer using carbon nanofibers–polydimethylsiloxane composite thin film. *Appl. Phys. Lett.* **2015**, *106*, 021902. [[CrossRef](#)]
57. Chang, W.Y.; Huang, W.; Kim, J.; Li, S.; Jiang, X. Candle soot nanoparticles–polydimethylsiloxane composites for laser ultrasound transducers. *Appl. Phys. Lett.* **2015**, *107*, 161903. [[CrossRef](#)]
58. Tian, J.; Zhang, Q.; Han, M. Distributed fiber-optic laser-ultrasound generation based on ghost-mode of tilted fiber Bragg gratings. *Opt. Express* **2013**, *21*, 6109–6114. [[CrossRef](#)] [[PubMed](#)]
59. Tian, Y.; Wu, N.; Zou, X.; Felemban, H.; Cao, C.; Wang, X. Fiber-optic ultrasound generator using periodic gold nanopores fabricated by a focused ion beam. *Opt. Eng.* **2013**, *52*, 065005. [[CrossRef](#)]
60. Tian, Y.; Wu, N.; Sun, K.; Zou, X.; Wang, X. Numerical simulation of fiber-optic photoacoustic generator using nanocomposite material. *J. Comput. Acoust.* **2013**, *21*, 1350002. [[CrossRef](#)]
61. Wu, N.; Sun, K.; Wang, X. Fiber optics photoacoustic generation using gold nanoparticles as target. *Proc. SPIE* **2011**, *798*, 765–768.
62. Wu, N.; Tian, Y.; Zou, X.; Wang, X. Fiber optic photoacoustic ultrasound generator based on gold nanocomposite. *Proc. SPIE* **2013**, 86940Q–86940Q-6.
63. Biagi, E.; Margheri, F.; Menichelli, D. Efficient laser-ultrasound generation by using heavily absorbing films as targets. *IEEE Trans. Ultrason. Ferroelectr. Freq. Control* **2001**, *48*, 1669–1680. [[CrossRef](#)] [[PubMed](#)]
64. Zou, X.; Schmittb, T.; Perloff, D.; Wu, N.; Yu, T.Y.; Wang, X. Nondestructive corrosion detection using fiber optic photoacoustic ultrasound generator. *Measurement* **2015**, *62*, 74–80. [[CrossRef](#)]
65. Roome, K.A.; Payne, P.A.; Dewhurst, R.J. Towards a sideways looking intravascular laser-ultrasound probe. *Sens. Actuators* **1999**, *76*, 197–202. [[CrossRef](#)]
66. Belsito, L. Design and Fabrication of MOMS-Based Ultrasonic Probes for Minimally Invasive Endoscopic Applications. Ph.D. Thesis, University of Bologna, Bologna, Italy, 2010.
67. Passler, K.; Nuster, R.; Gratt, S.; Burgholzer, P.; Paltauf, G. Laser-generation of ultrasonic X-waves using axicon transducers. *Appl. Phys. Lett.* **2009**, *94*, 064108. [[CrossRef](#)]
68. Baac, H.W.; Ling, T.; Ashkenazi, S.; Huang, S.W.; Guo, L.J. Photoacoustic concave transmitter for generating high frequency focused ultrasound. *Proc. SPIE* **2010**, 7564, 116.
69. Baac, H.W.; Ok, J.G.; Guo, L.J. Design of high-intensity focused ultrasound transmitters based on optoacoustic generation. In Proceedings of the 2011 IEEE International Ultrasonics Symposium, Orlando, FL, USA, 18–21 October 2011; pp. 2353–2356.
70. Lee, T.; Ok, J.G.; Youn, H.S.; Guo, L.J.; Baac, H.W. Micro-bubbles generated by a single focused optoacoustic wave. In Proceedings of the 2014 IEEE International Ultrasonics Symposium, Chicago, IL, USA, 3–6 September 2014; pp. 1041–1044.

71. Tong, L.H.; Lim, C.W.; Li, Y.C. Generation of high-intensity focused ultrasound by carbon nanotube opto-acoustic lens. *J. Appl. Mech.* **2014**, *81*, 081014. [[CrossRef](#)]
72. Chan, W.; Hies, T.; Ohl, C.D. Laser-generated focused ultrasound for arbitrary waveforms. *Appl. Phys. Lett.* **2016**, *109*, 174102. [[CrossRef](#)]
73. Buma, T.; Spisar, M.; O'Donnell, M. A high-frequency, 2-D array element using thermoelastic expansion in PDMS. *IEEE Trans. Ultrason. Ferroelectr. Freq. Control* **2003**, *50*, 1161–1176. [[CrossRef](#)] [[PubMed](#)]
74. Wu, N.; Tian, Y.; Zou, X.; Wang, X. Study of the compact fiber optic photoacoustic ultrasonic transducer. *Proc. SPIE* **2012**, *8345*, 83453Z–83453Z-10.
75. Schmieder, F.; Büttner, L.; Czarske, J. Adaptive laser-induced ultrasound generation using a micro-mirror array spatial light modulator. *Opt. Express* **2016**, *24*, 22536–22543. [[CrossRef](#)] [[PubMed](#)]
76. Biagi, E.; Cerbai, S.; Gambacciani, P.; Masotti, L. Fiber optic broadband ultrasonic probe. In Proceedings of the 7th IEEE Conference on Sensors, Lecce, Italy, 26–29 October 2008; pp. 363–366.
77. Colchester, R.J.; Zhang, E.Z.; Mosse, C.A.; Beard, P.C.; Papakonstantinou, I.; Desjardins, A.E. Broadband miniature optical ultrasound probe for high resolution vascular tissue imaging. *Biomed. Opt. Express* **2015**, *6*, 1502–1511. [[CrossRef](#)] [[PubMed](#)]
78. Zou, X.; Wu, N.; Tian, Y.; Zhang, Y.; Wang, X. Polydimethylsiloxane thin film characterization using all-optical photoacoustic mechanism. *Appl. Opt.* **2013**, *52*, 6239–6244. [[CrossRef](#)] [[PubMed](#)]
79. Kozhushko, V.V.; Hess, P. Nondestructive evaluation of microcracks by laser-induced focused ultrasound. *Appl. Phys. Lett.* **2007**, *91*, 224107. [[CrossRef](#)]
80. Kozhushko, V.V.; Hess, P. Laser-induced focused ultrasound for nondestructive testing and evaluation. *J. Appl. Phys.* **2008**, *103*, 124902. [[CrossRef](#)]
81. Karabutov, A.A.; Kaptil'nyi, A.G.; Ivochkin, A.Y. A laser optoacoustic method of inducing high-energy states and the investigation of phase transitions in metals at high pressures. *High Temp.* **2007**, *45*, 613–620. [[CrossRef](#)]
82. Xia, W.; Mosse, C.A.; Colchester, R.J.; Mari, J.M.; Nikitichev, D.I.; West, S.J.; Ourselin, S.; Beard, P.C.; Desjardins, A.E. Fiber optic photoacoustic probe with ultrasonic tracking for guiding minimally invasive procedures. *Proc. SPIE* **2015**, *13*, 244–248.
83. Sorazu, B.; Thursby, G.; Culshaw, B.; Dong, F.; Pierce, S.G.; Yang, Y.; Betz, D. Optical generation and detection of ultrasound. *Strain* **2003**, *39*, 111–114. [[CrossRef](#)]
84. Yao, J.; Wang, L.V. Sensitivity of photoacoustic microscopy. *Photoacoustics* **2014**, *2*, 87–101. [[CrossRef](#)] [[PubMed](#)]
85. Cai, D.; Li, Z.; Chen, S.L. In vivo deconvolution acoustic-resolution photoacoustic microscopy in three dimensions. *Biomed. Opt. Express* **2016**, *7*, 369–380. [[CrossRef](#)] [[PubMed](#)]
86. Chen, S.L.; Chang, Y.C.; Zhang, C.; Ok, J.G.; Ling, T.; Mihnev, M.T.; Norris, T.B.; Guo, L.J. Efficient real-time detection of terahertz pulse radiation based on photoacoustic conversion by carbon nanotube nanocomposite. *Nat. Photonics* **2014**, *8*, 537–542. [[CrossRef](#)]
87. Zhang, C.; Chen, S.L.; Ling, T.; Guo, L.J. Imprinted polymer microrings as high-performance ultrasound detectors in photoacoustic imaging. *IEEE J. Lightw. Technol.* **2015**, *33*, 4318–4328. [[CrossRef](#)]
88. Yoo, G.; Yoon, H.; Heo, J.; Thakur, U.K.; Park, H.J.; Baac, H.W.; Heo, J. All-optical ultrasound transducer using CNT-PDMS and etalon thin-film structure. *IEEE Photonics J.* **2015**, *7*, 6903708. [[CrossRef](#)]
89. Hou, Y.; Ashkenazi, S.; Huang, S.W.; O'Donnell, M. An integrated optoacoustic transducer combining etalon and black PDMS structures. *IEEE Trans. Ultrason. Ferroelectr. Freq. Control* **2008**, *55*, 2719–2725. [[PubMed](#)]
90. Noimark, S.; Colchester, R.J.; Blackburn, B.J.; Zhang, E.Z.; Alles, E.J.; Ourselin, S.; Beard, P.C.; Papakonstantinou, I.; Parkin, I.P.; Desjardins, A.E. Carbon-nanotube–PDMS composite coatings on optical fibers for all-optical ultrasound imaging. *Adv. Funct. Mater.* **2016**. [[CrossRef](#)]
91. Cai, D.; Li, Z.; Chen, S.L. Photoacoustic microscopy by scanning mirror-based synthetic aperture focusing technique. *Chin. Opt. Lett.* **2015**, *13*, 101101. [[CrossRef](#)]
92. Miida, Y.; Matsuura, Y. All-optical photoacoustic imaging system using fiber ultrasound probe and hollow optical fiber bundle. *Opt. Express* **2013**, *21*, 22023–22033. [[CrossRef](#)] [[PubMed](#)]
93. Alles, E.J.; Noimark, S.; Zhang, E.; Beard, P.C.; Desjardins, A.E. Pencil beam all-optical ultrasound imaging. *Biomed. Opt. Express* **2016**, *7*, 3696–3704. [[CrossRef](#)] [[PubMed](#)]
94. Biagi, E.; Cerbai, S.; Masotti, L.; Belsito, L.; Roncaglia, A.; Masetti, G.; Speciale, N. Fiber optic broadband ultrasonic probe for virtual biopsy: Technological solutions. *J. Sens.* **2010**, *2010*, 917314. [[CrossRef](#)]

95. Sheaff, C.; Ashkenazi, S. A polyimide-etalon thin film structure for all-optical high-frequency ultrasound transduction. *IEEE Trans. Ultrason. Ferroelectr. Freq. Control* **2012**, *59*, 2254–2261. [[CrossRef](#)] [[PubMed](#)]
96. Sheaff, C.; Ashkenazi, S. Characterization of an improved polyimide-etalon all-optical transducer for high-resolution ultrasound imaging. *IEEE Trans. Ultrason. Ferroelectr. Freq. Control*. **2014**, *61*, 1223–1232. [[CrossRef](#)] [[PubMed](#)]
97. Alles, E.J.; Colchester, R.J.; Desjardins, A.E. Adaptive light modulation for improved resolution and efficiency in all-optical pulse-echo ultrasound. *IEEE Trans. Ultrason. Ferroelectr. Freq. Control* **2016**, *63*, 83–90. [[CrossRef](#)] [[PubMed](#)]
98. Zhang, E.; Laufer, J.; Beard, P. Backward-mode multiwavelength photoacoustic scanner using a planar Fabry-Perot polymer film ultrasound sensor for high-resolution three-dimensional imaging of biological tissues. *Appl. Opt.* **2008**, *47*, 561–577. [[CrossRef](#)] [[PubMed](#)]
99. Chen, S.L.; Guo, L.J.; Wang, X. All-optical photoacoustic microscopy. *Photoacoustics* **2015**, *3*, 143–150. [[CrossRef](#)]
100. Hsieh, B.Y.; Chen, S.L.; Ling, T.; Guo, L.J.; Li, P.C. All-optical scanhead for ultrasound and photoacoustic dual-modality imaging. *Opt. Express* **2012**, *20*, 1588–1596. [[CrossRef](#)] [[PubMed](#)]
101. Nuster, R.; Schmitner, N.; Wurzinger, G.; Gratt, S.; Salvenmoser, W.; Meyer, D.; Paltauf, G. Hybrid photoacoustic and ultrasound section imaging with optical ultrasound detection. *J. Biophotonics* **2013**, *6*, 549–559. [[CrossRef](#)] [[PubMed](#)]
102. Hsieh, B.Y.; Chen, S.L.; Ling, T.; Guo, L.J.; Li, P.C. All-optical scanhead for ultrasound and photoacoustic imaging-Imaging mode switching by dichroic filtering. *Photoacoustics* **2014**, *2*, 39–46. [[CrossRef](#)] [[PubMed](#)]
103. Colchester, R.J.; Mosse, C.A.; Nikitichev, D.I.; Zhang, E.Z.; West, S.; Beard, P.C.; Papakonstantinou, I.; Desjardins, A.E. Real-time needle guidance with photoacoustic and laser-generated ultrasound probes. *Proc. SPIE* **2015**, 9323. [[CrossRef](#)]
104. Dehoux, T.; Abi Ghanem, M.; Zouani, O.F.; Rampnoux, J.M.; Guillet, Y.; Dilhaire, S.; Durrieu, M.C.; Audoin, B. All-optical broadband ultrasonography of single cells. *Sci. Rep.* **2015**, *5*, 8650. [[CrossRef](#)] [[PubMed](#)]
105. Colchester, R.J.; Noimark, S.; Mosse, C.A.; Zhang, E.Z.; Beard, P.C.; Parkin, I.P.; Papakonstantinou, I.; Desjardins, A.E. All-optical pulse-echo ultrasound probe for intravascular imaging (Conference Presentation). *Proc. SPIE* **2016**, 9689. [[CrossRef](#)]
106. Decremps, F.; Gauthier, M.; Ayrinhac, S.; Bove, L.; Belliard, L.; Perrin, B.; Morand, M.; Marchand, G.L.; Bergame, F.; Philippe, J. Picosecond acoustics method for measuring the thermodynamical properties of solids and liquids at high pressure and high temperature. *Ultrasonics* **2015**, *56*, 129–140. [[CrossRef](#)] [[PubMed](#)]
107. Majlesi, J.; Unalan, H. High-power pain threshold ultrasound technique in the treatment of active myofascial trigger points: A randomized, double-blind, case-control study. *Arch. Phys. Med. Rehabil.* **2004**, *85*, 833–836. [[CrossRef](#)] [[PubMed](#)]
108. Dong, B.; Chen, S.; Zhang, Z.; Sun, C.; Zhang, H.F. Photoacoustic probe using a microring resonator ultrasonic sensor for endoscopic applications. *Opt. Lett.* **2014**, *39*, 4372–4375. [[CrossRef](#)] [[PubMed](#)]
109. Stasio, N.; Shibukawa, A.; Papadopoulos, I.N.; Farahi, S.; Simandoux, O.; Huignard, J.P.; Bossy, E.; Moser, C.; Psaltis, D. Towards new applications using capillary waveguides. *Biomed. Opt. Express* **2015**, *6*, 4619–4631. [[CrossRef](#)] [[PubMed](#)]

